Optical and Quantum Electronics (2018) 50:373
https://doi.org/10.1007/s11082-018-1639-1

Optimization of cubic GaN/AlGaN quantum cascade structures for negative refraction in the THz spectral range

Miloš Dubajić[1,2] · Aleksandar Daničić[3] · Nikola Vuković[1] · Vitomir Milanović[1] · Jelena Radovanović[1]

Received: 29 May 2018 / Accepted: 22 September 2018 / Published online: 28 September 2018

Abstract
In this work we theoretically investigate a possibility to use cubic nitride based multi-layer periodic nanostructure as a semiconductor metamaterial. The structure design is based on an active region of a quantum cascade laser optimized to achieve optical gain in the Terahertz (THz) spectral range. In particular, we test the GaN/AlGaN quantum well configurations, which should exhibit important advantages compared to GaAs-based structures, namely room temperature operation without the assistance of magnetic field and lower doping densities. Our numerical rate-equations model is solved self-consistently and it takes into account electron-longitudinal optical phonon scattering between all the relevant states among the adjacent periods of the structure. A global optimization routine, specifically genetic algorithm is then used to generate new gain-optimized structures. This work confirms the advantages of cubic GaN designs over GaAs ones, namely feasibility of negative refraction at room temperature without the assistance of magnetic field while keeping the doping densities of the same order of magnitude.

Keywords Quantum cascade structure · Semiconductor metamaterials · Negative refraction

This article is part of the Topical Collection on Focus on Optics and Bio-photonics, Photonica 2017.

Guest Edited by Jelena Radovanovic, Aleksandar Krmpot, Marina Lekic, Trevor Benson, Mauro Pereira, Marian Marciniak.

✉ Nikola Vuković
nikolavukovic89@gmail.com

[1] School of Electrical Engineering, University of Belgrade, Bulevar Kralja Aleksandra 73, Belgrade 11120, Serbia

[2] School of Photovoltaic and Renewable Energy Engineering, University of New South Wales, Sydney 2052, Australia

[3] Vinča Institute of Nuclear Sciences, University of Belgrade, P.O.B. 522, Belgrade 11001, Serbia

1 Introduction

Artificial periodic electromagnetic composites known as metamaterials (MTMs), which manifest properties not attainable with naturally existing structures, including negative refraction, near-zero permittivity etc., have been increasingly investigated during the past decade (Chen et al. 2006; Ginzburg and Orenstein 2008; Schurig et al. 2006). The main idea is to optimally engineer effective medium parameters such as permeability and permittivity in order to control transmission and reflection of electromagnetic waves in a desirable manner.

The first demonstration of negative index media was performed at microwave frequencies (Shelby et al. 2001), followed by a demonstration of metamaterials operating at near-infrared (NIR) and visible frequencies (Grigorenko et al. 2005; Zhou et al. 2005). Those structures were based on double resonance approach (i.e. the proper operation required both permittivity and permeability to be simultaneously negative). However, it was indicated that other mechanism could also lead to negative refraction (in this case only for TM polarized electric field modes) if material exhibited optical anisotropy (Podolskiy and Narimanov 2005). The factor which determines MTMs performance and limits their usefulness, along with the complexity of fabrication process, is significant optical loss caused by metallic films, spheres or wires which are in most cases constitutive parts of the proposed and experimentally demonstrated structures (Shalaev 2007). Inspired by the theoretical work of Podolskiy who proposed anisotropy as means for achieving negative refraction, and with the aim to exclude metallic inclusions, the first all-semiconductor metamaterial structure operating at long-wave infrared region was developed (Hoffman et al. 2007). Since then, an extremely strong anisotropy was utilized to design new type of materials named hyperbolic materials (Liu et al. 2007; Thongrattanasiri and Podolskiy 2009), where the most recent approaches assumed all-semiconductor configuration (Desouky et al. 2017; Feng et al. 2017). One direction of semiconductor metamaterials research targets further reduction of losses, which are still present in semiconductors, by introducing low-dimensional semiconductor quantum structures. In this case, the losses are compensated by the gain obtained through NIR and mid-infrared (MIR) intersubband transitions in quantum cascade laser (QCL)-like structures (Ginzburg and Orenstein 2008).

Following the rapid development of THz QCLs with large spectral coverage of 1.2–4.9 THz (Vitiello et al. 2015), our previous efforts were focused on semiconductor metamaterials based on GaAs/AlGaAs THz QCL designs (Daničić et al. 2016; Radovanović et al. 2012; Vuković et al. 2015). However, the main drawbacks of the proposed approaches were the necessity for a strong magnetic field and high values of the total electron sheet density required for operation. The idea to replace GaAs platform with nitrides would potentially result in lowering of the required doping densities and increasing of the operating temperatures (Ginzburg and Orenstein 2008). Namely, doping density may be reduced since the average permittivity of the background material is lower for GaN and longitudinal optical phonon energy is higher at room temperature (see also Sect. 2). Taking into account that nitrides with wurtzite crystal structure possess a large spontaneous polarization and piezoelectric constant, resulting in a strong built-in electric fields (Fiorentini et al. 2002), we instead choose to consider only cubic (zinc-blende) crystal structure. In this paper, we therefore take into account the design of semiconductor metamaterial based on cubic GaN/AlGaN QCL-like structure for application in the THz spectral range, which is supposed to deliver sufficient amount of optical gain to achieve negative refraction without the assistance of magnetic field, at room temperature. Our calculations are based on the system of

rate-equations, which is solved self-consistently to evaluate the carrier densities, while the GA for global optimization is used to generate new structures with optimized gain. This communication is organized as follows: Sect. 2 provides brief description of the model, in Sect. 3 we present results of numerical simulations for two optimized structures and Sect. 4 concludes the paper with a brief closing summary.

2 Theoretical considerations

Quantum cascade laser is a low-dimensional semiconductor structure that consists of series of identical stages. When the structure is biased by an external electric field, electron transported along the growth direction can, in ideal conditions, emit as many photons as the number of periods (Faist et al. 1994). The design of such device assumes careful positioning of electronic subbands defined as the upper and the lower laser state (between which the radiative transitions occur), electric pumping along the growth direction, as well as creating an array of these active regions responsible for light amplification. Dynamical properties show significant difference from interband lasers, as non-radiative intersubband scattering mechanisms are very fast, reaching values of several picoseconds (Wacker 2012). The possibility of changing the lasing wavelength in semiconductor quantum well-based lasers (in particular QCLs) by modifying the layer widths, while retaining the same material composition, proves as essential when it comes to choosing the active medium for possible MTM realizations. Specifically, by tuning the transition resonant frequency it is possible to efficiently engineer effective permittivity of the structure. The permeability of a semiconductor-based nonmagnetic metamaterial is $\mu = 1$, while the intersubband induced permittivity for the quantum structure unit cell, considering strong anisotropy of optical properties, is represented by the dielectric permittivity tensor that has the following form (Ginzburg and Orenstein 2008):

$$\varepsilon = \begin{bmatrix} \varepsilon_{\parallel} & 0 & 0 \\ 0 & \varepsilon_{\parallel} & 0 \\ 0 & 0 & \varepsilon_{\perp} \end{bmatrix} \tag{1}$$

where $\varepsilon_x = \varepsilon_y = \varepsilon_{\parallel}$ is the permittivity component along the quantum well planes (perpendicular to the growth direction z) and is equal to ε_b-the averaged permittivity of the background material. Permittivity along the growth axes (z), denoted by $\varepsilon_{\perp}$, is described by the Lorenzian model (Basu 2003):

$$\varepsilon_{\perp}(\omega) = \varepsilon_b + \frac{1}{L_p}\frac{e^2}{\varepsilon_0 \hbar}\sum_{n>m}\left(N_{s,m} - N_{s,n}\right)\left[\frac{|z_{mn}|^2}{(\omega_{nm} - \omega) - i\gamma_{nm}} + \frac{|z_{mn}|^2}{(\omega_{nm} + \omega) + i\gamma_{nm}}\right] \tag{2}$$

Here, L is the length of the unit cell in the z direction, $N_{s,i}$ represents the electron sheet density in the i-th state, $\omega_{nm} = \frac{(E_n - E_m)}{\hbar} > 0$, when $n > m$, is the resonant transition frequency between states n and m, ω stands for the frequency of the input light, γ_{nm} denotes the transition linewidth between states n and m which is set to be $\gamma = 2$ meV and same for all transitions considered (Daničić et al. 2016), while z_{mn} is the transition matrix element between states n and m. Antiresonant term on the right hand side of Eq. (2) containing $\omega_{nm} + \omega + i\gamma_{nm}$ can be justifiably neglected in all cases near resonance. In general, it is possible to write an analog expression to Eq. (2) when summation goes for $n < m$, however

that expression is hardly ever used. In order to achieve negative refraction, we must satisfy specific criteria, which in case of anisotropic, single-negative MTM read (Podolskiy and Narimanov 2005):

$$Re(\varepsilon_{\perp}) < 0, \quad \varepsilon_{\parallel} > 0 \tag{3}$$

We decompose the complex permittivity from Eq. (2) into its real and imaginary part:

$$Re(\varepsilon_{\perp}) = \varepsilon_b + \frac{1}{L_p}\frac{e^2}{\varepsilon_0 \hbar}\sum_{n,m}\left(N_{s,m} - N_{s,n}\right)\frac{\left|z_{mn}\right|^2\left(\omega_{nm} - \omega\right)}{\left(\omega_{nm} - \omega\right)^2 + \gamma_{nm}^2} \tag{4}$$

$$Im(\varepsilon_{\perp}) = \frac{1}{L_p}\frac{e^2}{\varepsilon_0 \hbar}\sum_{n,m}\left(N_{s,m} - N_{s,n}\right)\frac{\left|z_{mn}\right|^2\gamma_{nm}}{\left(\omega_{nm} - \omega\right)^2 + \gamma_{nm}^2} \tag{5}$$

and recall that the negative imaginary part represents the gain, while the positive imaginary part implies attenuation. If we assume that a particular transition is the dominant one (e.g. between the upper and the lower laser state) and that we have a high enough value of the transition matrix element z_{nm}, it is obvious that depending on the sign of $\left(N_{s,n} - N_{s,m}\right)$, where $n < m$, we can have both passive $\left(N_{s,n} - N_{s,m}\right) > 0$ or active configuration $\left(N_{s,n} - N_{s,m}\right) < 0$ (the case when population inversion is achieved). To reach the goal defined previously, i.e. negative refraction in a specific spectral range, compensating the losses by stimulated light amplification, vital condition is to produce high population inversion.

The carrier dynamics in the active region is dominated by electron-LO phonon interactions which provide extremely fast depopulation of the lower laser state and consequently enhance the population inversion. Critical drawback of GaAs candidates for efficient negative refraction in the THz range at room temperature is the following: the resonant LO phonon energy (36 meV) is relatively small and comparable to room temperature thermal energy $k_bT = 26$ meV. Consequently, a large percentage of electrons with high kinetic energies relax from the upper laser state to the lower laser state by electron-LO phonon scattering and therefore undermine the population inversion. In addition, low GaAs LO phonon energy increases the thermal population of the lower laser state which again deteriorates the population inversion. Conversely, GaN based QCL-like structure has the advantage of higher LO phonon resonant energy which is 87.3 meV at 300 K (Levinshteĭn et al. 2001).

The modelling of electron transport is performed by setting up a full set of rate equations which must be solved self-consistently. Electron-LO-phonon scattering rate without the magnetic field is calculated following the approaches described in Smiljanić et al. (2014), Unuma et al. (2001). We presume that electron-LO phonon scattering is by far the most dominant process for the particular structures considered in the present work and neglect the interface roughness contribution. Assuming one period with a set of N states, each corresponding to an electron subband originating from quantum confinement in multiple quantum wells of QCL, and considering a central period with its P nearest neighbours, scattering rate equations in the equilibrium can be written as (Mirčetić et al. 2005):

$$\sum_{j=1,j\neq i}^{N} n_j W_{j,i} - n_i \sum_{j=1,j\neq i}^{N} W_{i,j} + \sum_{k=1}^{P}\sum_{j=1,j\neq i}^{N}\left[n_j\left(W_{j,i+kN} + W_{j+kN,i}\right) - n_i\left(W_{i+kN,j} + W_{i,j+kN}\right)\right] = 0 \tag{6}$$

where $i + kN$ is the ith state of the kth neighbouring period, $W_{i,j}$ is the total scattering rate from ith into jth state, and n_i is the electron density in the ith state. The first two sums in Eq. (6) are due to intraperiod scattering while the third is a consequence of interperiod scattering. One has to take into account that the electron distribution in each subband is defined by the Fermi–Dirac function with a particular value of the quasi-Fermi level, hence the scattering rates need to be averaged according to the following expression (Harrison and Valavanis 2016):

$$W_{i,j} = \frac{\int_{E_{i0}}^{+\infty} \tilde{W}_{i,j} f_i^{FD}(E_i)[1 - f_j^{FD}(E_i - \hbar\omega_{LO})]dE_i}{\int_{E_{i0}}^{+\infty} f_i^{FD}(E_i)dE_i} \tag{7}$$

where $E_i = E_{i0} + \frac{(\hbar k_t)^2}{2m_i^*}$ represents the energy of ith (initial) state in parabolic approximation $\tilde{W}_{i,j}$ scattering rate between ith and jth (final) state as a function of transversal wave vector k_t of ith state, $f_{i,j}^{FD}(E_{i,j}) = \frac{1}{exp\left(\left(E_{i,j} - E_{F_{i,j}}\right)/(k_b T)\right)+1}$ is Fermi–Dirac distribution of ith or jth state at room temperature (T = 300 K), where quasi-Fermi energies can be calculated using:

$$n_{i,j} = \frac{1}{2\pi}\int_0^{+\infty} f_{i,j}^{FD}(k_t^2)d(k_t^2) = \frac{k_b T m_{i,j}^*}{\pi\hbar^2}\ln\left(1 + e^{\frac{E_{Fi,j} - E_{i0,j0}}{k_b T}}\right) = \frac{m_{i,j}^*}{\pi\hbar^2}\int_{E_{i0,j0}}^{+\infty} f_{i,j}^{FD}(E_{i,j})dE_{i,j} \tag{8}$$

It is evident from Eqs. (7) and (8) that the scattering rates which enter the system (6) depend upon the carrier densities and it is therefore necessary to solve Eq. (6) self-consistently in order to calculate the values of $\varepsilon_\perp$.

3 Results and discussion

Numerical calculations in this Section are performed for cubic GaN/AlGaN based quantum cascade laser-like structures, designed to emit radiation at THz frequencies. In order to minimize the number of quantum wells in QCL and obtain the close packing of the active regions our approach is to fix the number of quantum wells to three per period (Luo et al. 2007) and then to use the genetic algorithm to gain-optimize the structure. Two types of structures will be analyzed with different constraints applied in the optimization process. A shooting method solver was used to find the energies and wave functions for the structures. Specifically, energies and related wave functions were calculated for the structure with 9 QWs (3 periods) in order to extract results for the middle period which would be used as relevant input for the calculations. This was done particularly in order to ensure that electronic band structure is not affected by boundary effects making it close to the structure of realistic QCL where number of periods is very large. Following this, the self-consistent scattering rates calculations, state populations and quasi-Fermi energy calculations were performed to give self-consistent subband carrier densities which impact the permittivity function. Conduction band nonparabolicity is taken into account as in Ekenberg (1989), Vuković et al. (2014a, b).

The main goal of the work is to optimize the structures to behave like left-handed semiconductor metamaterials while keeping the carrier sheet densities required for fulfilling the

negative refraction condition, given by Eq. (3), to realistic values. For that reason the lasing transition energy was not fixed to an exact value during the optimization procedure but only constrained to values within the THz spectral range. The fitness function used is represented by Eq. (9). The structures obtained in this calculation may indicate the practical minima of doping levels which provide negative refraction for cubic GaN/AlGaN quantum cascade laser structures. It is then straightforward to repeat the process for predefined transition energy, but allowing larger sheet densities, Eq. (10).

For that purpose the previously mentioned GA will be used, which is a stochastic method inspired by natural selection rules from Darwin's theory of evolution, which aims to find the optimal set of parameters that will maximize the given target (fitness) function. For the purpose of this paper, in order to attain negative refraction, the target function must involve $Re\{\varepsilon_{\perp}([d,K,x])\}$ where $[d,K,x]$ is the set of parameters that we want to optimize, which contains $d = [d_{w1}, d_{b1}, \ldots, d_{w(n-1)}, d_{b(n-1)}, d_{wn}]$, set of barrier and well thicknesses in one period, in our particular case set to be $n = 3$, K is the electric field applied to the structure and x is the molar fraction of AlN in AlGaN barrier alloy. The parameters of the GA that have to be set and which define the effectiveness of the search are: population size, number of elite individuals, crossover and mutation. In short, the first step in algorithm is to create the population from set initial values of the parameters that are to be optimized. Random mutations are subsequently applied (in a predefined percentage) to the population members, namely, values in sets that define 'an individual' are randomly changed. For each set of parameters (each individual) the fitness function is evaluated and a specific number of individuals (set by elitism parameter) that have the best values of 'fitness' are directly kept for the next iteration. Before going to a new iteration (the formation of next generation) crossover is applied to a number of remaining individuals which simulates the interchange of genetic material. Thus, a new population is generated and the same process is repeated until convergence criteria are satisfied. The following fitness functions are used in this work:

$$F = \begin{cases} \min\{Re(\varepsilon_{\perp})\}, & Re(\varepsilon_{\perp}) < 0\, Im(\varepsilon_{\perp}) < 0 \\ c, & Re(\varepsilon_{\perp}) > 0\, Im(\varepsilon_{\perp}) > 0 \end{cases} \tag{9}$$

$$F = \begin{cases} \min\{Re(\varepsilon_{\perp})\}\left|Im\{Re[\varepsilon_{\perp}(\omega_L)]\}\right|, & Re(\varepsilon_{\perp}) < 0\, Im(\varepsilon_{\perp}) < 0 \\ c, & Re(\varepsilon_{\perp}) > 0\, Im(\varepsilon_{\perp}) > 0 \end{cases} \tag{10}$$

where c is an arbitrary large positive constant which ensures divergence when condition of negative refraction and gain are not achieved, i.e. when $Re(\varepsilon_{\perp}) < 0\, Im(\varepsilon_{\perp}) < 0$ (in our case we are searching for the minimum of F function, i.e. the elite individuals are individuals that give the lowest value of fitness function), and ω_L is the lasing frequency which can be set precisely (in our case $\omega_L = 6.26$ THz). Equation (9) represent the case when we are looking for negative refraction in the THz range and Eq. (10) is the fitness function for the negative refraction with additional condition, i.e. specific lasing frequency, while in both cases gain condition must be satisfied.

The material parameters used in our numerical calculations are: $m_{GaN} = 0.11 m_0$ (Machhadani et al. 2011), $m_{AlN} = 0.33 m_0$ (Westmeyer et al. 2006), $E_{gGaN} = 3.45$ eV, $E_{gAlN} = 6.7$ eV (Machhadani et al. 2011). The GaN/AlN conduction band offset was taken as $\Delta E_c = 1.6$ eV (Machhadani et al. 2011).

The first structure, designed to have optical transition within the THz spectral range, is realized on $GaN/Al_{0.1}Ga_{0.9}N$ platform emitting at 1.96 THz. The structural parameters can

be seen in Fig. 1a where the borders of one period are indicated by a dashed rectangle, with layer widths amounting to 37Å, 65Å, 16Å, 8 Å, 54Å, 27Å (starting from the left well), and $U_B = 0.16$ eV (the barrier height). The applied electric field in the z-direction is K = 56 kV/cm. The energy difference between subbands 3 and 2 is 8.1 meV corresponding to 1.96 THz (153 μm), while the difference between the lower laser state and the ground state was directed by GA towards the LO phonon energy (87.3 meV) and reached 83 meV.

From Fig. 1a, one can see that our structure provided by GA exploits the standard mechanism for injecting carriers between periods. Radiative transition which occurs between levels 3 and 2 is diagonal, which leads to a longer upper-laser-state lifetime and larger population inversion. Fast depopulation of lower-laser-state (2) to the ground-laser-state (1) is achieved by electron LO phonon scattering.

In Fig. 1b we present the $GaN/Al_{0.11}Ga_{0.89}N$ QCL structure optimized for lasing at 6.26 THz. Layers' widths are 32 Å, 49 Å, 27 Å, 44 Å, 21 Å, 41 Å (starting from the left well), and barrier height is $U_B = 0.18$ eV. The applied electric field in the z-direction is K = 52 kV/cm. Energy difference between the subbands 3 and 2 is 26 meV which corresponding to 6.26 THz (48 μm). We have started the optimization process using the same three well per period design of the structure, however, the conduction band profile has converged to a somewhat different case where the electron-LO phonon scattering mechanism is responsible for the transfer of electrons from the ground-state of one period into the top-state of the next period. Here, the depopulation of the lower-state is facilitated by sufficient overlap between wave functions of lower and ground state.

GA searches for the optimal structural parameters of the QCL like structure by iteratively evaluating $\varepsilon_\perp$ function for the chosen N_s value until it converges toward negative values for certain (free or constrained) frequency range. Target function in form of $\varepsilon_\perp$ can be calculated from Eqs. (4) and (5), by obtaining the distribution of carriers among the states of the structure, i.e. by solving self-consistently the system (6) [using Eqs. (7) and (8)]. Figure 2 illustrates the critical values of the total sheet carrier density for which we achieve negative refraction for the two different structures considered in this paper. In order to determine the minimum doping density alongside the frequency range of negative refraction (Δf), for an active metamaterial we have to be sure that both $Re(\varepsilon_\perp) < 0$ and $Im(\varepsilon_\perp) < 0$, (latter is condition of having gain and thus obtaining the active medium which will compensate losses in the structure). Note that increase in doping density results in increase of both Δf and minimum values of $Re(\varepsilon_\perp)$ and $Im(\varepsilon_\perp)$. For example, for $N_s = 2.5 \times 10^{12}$ cm^{-2} the structure depicted in Fig. 1a has $\varepsilon_R < 0$ and $\varepsilon_I < 0$ for a rather wide range Δf with maximum frequency of 1.4 THz. However, achieving negative refraction for

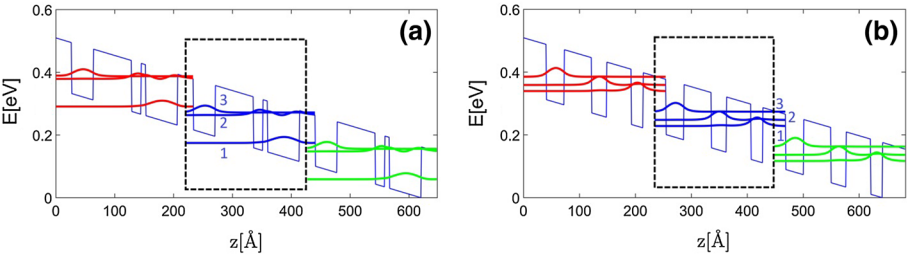

Fig. 1 The conduction-band diagram of QCL-like structure (three periods are shown) designed for lasing at **a** 1.96 THz and **b** 6.26 THz. A single period of each structure is enclosed by a dashed rectangle

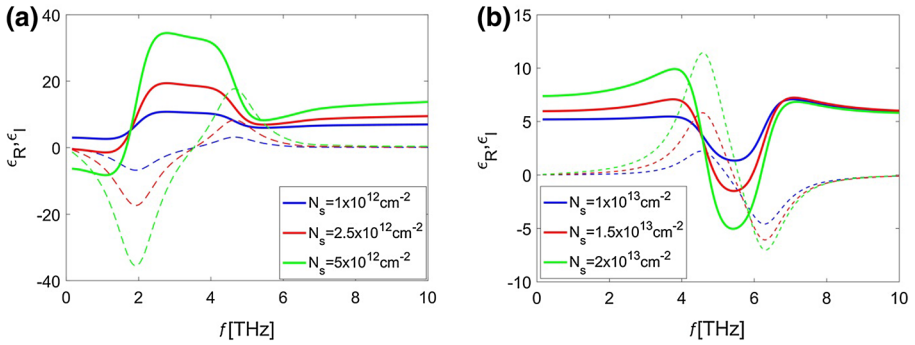

Fig. 2 The dependence of real part of $\varepsilon_{\perp}(\varepsilon_R$, full lines) and the imaginary part (ε_I, dashed lines) on frequency f for various values of total sheet carrier density in case of a structure designed for **a** $f=1.96$ THz and **b** $f=6.26$ THz transition

structure in Fig. 1b requires significantly higher doping densities of around $N_s=1.5\times10^{13}$ cm^{-2}, frequency range Δf is limited to 0.5 THz (the maximum frequency is limited by the constraint of $\varepsilon_I < 0$ and amounts to 5.7 THz for all N_s). Further increase of N_s will decrease the minimum frequency, thus increasing Δf while keeping maximum frequency constant as mentioned above. It is important to emphasize that this structure is not designed as an actual laser but it can rather be interpreted as a QCL like structure that is used in order to realize gain for a range of frequencies where the negative refraction occurs (in order to compensate the losses). The "laser transition" takes place between the energy states whose energy difference relates to frequency f_g for which minimum of $Im(\varepsilon_{\perp})$ (Fig. 2 dashed curves) is achieved (at 1.96 THz and 6.26 THz in Fig. 2a, b respectively).

However, the central frequency f_r for negative refraction range Δf (the frequency f_r relates to the minimum of $(\varepsilon_{\perp})$) and the gain frequency f_g do not necessarily coincide ($f_{r1}=1.8$ THz, $f_{r2}=5.5$ THz while $f_{g1}=1.96$ THz, $f_{g2}=6.26$ THz as per Fig. 2).

4 Conclusion

Based on our numerical simulations we predict that novel structures realized in cubic GaN/AlGaN could be used as active media for semiconductor based metamaterials, providing negative refraction in the THz spectral range at room temperatures. Comparing the two structures that we considered in this work one can conclude that the theoretical minimum of sheet concentration for triple well per period GaN/AlGaN QCL design is $N_s=2.5\times10^{12}$ cm^{-2} at 1.8 THz, while increase in lasing frequency leads to higher doping densities.

Nitrides-focused QCL design has shown to be very promising in comparison to GaAs/AlGaAs QCL material system, therefore our future work will include the effort to further extend the negative permittivity frequency range while employing the same GaN/AlGaN platform, by changing the number of wells per period and expanding the model to include additional scattering mechanisms.

Acknowledgements The authors acknowledge support from COST ACTION MP1204 (TERA-MIR Radiation: Materials, Generation, Detection and Applications), COST ACTION MP1406 (MultiscaleSolar—Multiscale in modelling and validation for solar photovoltaics) and Ministry of Education, Science and

Technological Development (Republic of Serbia), ev. no. III 45010, as well as UNSW for the use of high-performance computing facilities.

References

Basu, P.K.: Theory of Optical Processes in Semiconductors. Oxford University Press, Oxford (2003)

Chen, H.-T., Padilla, W.J., Zide, J.M.O., Gossard, A.C., Taylor, A.J., Averitt, R.D.: Active terahertz metamaterial devices. Nature **444**, 597–600 (2006). https://doi.org/10.1038/nature05343

Daničić, A., Radovanović, J., Ramović, S., Milanović, V.: Exploring negative refraction conditions for quantum cascade semiconductor metamaterials in the terahertz spectral range. J. Phys. D Appl. Phys. **49**, 085105 (2016). https://doi.org/10.1088/0022-3727/49/8/085105

Desouky, M., Mahmoud, A.M., Swillam, M.A.: Tunable mid IR focusing in InAs based semiconductor hyperbolic metamaterial. Sci. Rep. **7**, 15312 (2017). https://doi.org/10.1038/s41598-017-15493-4

Ekenberg, U.: Nonparabolicity effects in a quantum well: sublevel shift, parallel mass, and Landau levels. Phys. Rev. B **40**, 7714–7726 (1989). https://doi.org/10.1103/PhysRevB.40.7714

Faist, J., Capasso, F., Sivco, D.L., Sirtori, C., Hutchinson, A.L., Cho, A.Y.: Quantum cascade laser. Science **264**, 553–556 (1994). https://doi.org/10.1126/science.264.5158.553

Feng, K., Harden, G., Sivco, D.L., Hoffman, A.J.: Subdiffraction confinement in all-semiconductor hyperbolic metamaterial resonators. ACS Photon. **4**, 1621–1626 (2017). https://doi.org/10.1021/acsphotonics.7b00309

Fiorentini, V., Bernardini, F., Ambacher, O.: Evidence for nonlinear macroscopic polarization in III–V nitride alloy heterostructures. Appl. Phys. Lett. **80**, 1204–1206 (2002). https://doi.org/10.1063/1.1448668

Ginzburg, P., Orenstein, M.: Metal-free quantum-based metamaterial for surface plasmon polariton guiding with amplification. J. Appl. Phys. **104**, 063513 (2008). https://doi.org/10.1063/1.2978208

Grigorenko, A.N., Geim, A.K., Gleeson, H.F., Zhang, Y., Firsov, A.A., Khrushchev, I.Y., Petrovic, J.: Nanofabricated media with negative permeability at visible frequencies. Nature **438**, 335–338 (2005). https://doi.org/10.1038/nature04242

Harrison, P., Valavanis, A.: Quantum Wells, Wires and Dots. Wiley, Chichester (2016)

Hoffman, A.J., Alekseyev, L., Howard, S.S., Franz, K.J., Wasserman, D., Podolskiy, V.A., Narimanov, E.E., Sivco, D.L., Gmachl, C.: Negative refraction in semiconductor metamaterials. Nat. Mater. **6**, 946–950 (2007). https://doi.org/10.1038/nmat2033

Levinshteĭn, M.E., Mikhail, E., Shur, M., Rumyantsev, S.L.: Properties of Advanced Semiconductor Materials: GaN, AlN, InN, BN, SiC, SiGe. Wiley, New York (2001)

Liu, Z., Lee, H., Xiong, Y., Sun, C., Zhang, X.: Far-field optical hyperlens magnifying sub-diffraction-limited objects. Science **315**, 1686 (2007). https://doi.org/10.1126/science.1137368

Luo, H., Laframboise, S.R., Wasilewski, Z.R., Aers, G.C., Liu, H.C., Cao, J.C.: Terahertz quantum-cascade lasers based on a three-well active module. Appl. Phys. Lett. **90**, 041112 (2007). https://doi.org/10.1063/1.2437071

Machhadani, H., Tchernycheva, M., Sakr, S., Rigutti, L., Colombelli, R., Warde, E., Mietze, C., As, D.J., Julien, F.H.: Intersubband absorption of cubic GaN/Al(Ga)N quantum wells in the near-infrared to terahertz spectral range. Phys. Rev. B **83**, 075313 (2011). https://doi.org/10.1103/PhysRevB.83.075313

Mirčetić, A., Indjin, D., Ikonić, Z., Harrison, P., Milanović, V., Kelsall, R.W.: Towards automated design of quantum cascade lasers. J. Appl. Phys. **97**, 084506 (2005). https://doi.org/10.1063/1.1882768

Podolskiy, V.A., Narimanov, E.E.: Strongly anisotropic waveguide as a nonmagnetic left-handed system. Phys. Rev. B **71**, 201101 (2005). https://doi.org/10.1103/PhysRevB.71.201101

Radovanović, J., Ramović, S., Daničić, A., Milanović, V.: Negative refraction in semiconductor metamaterials based on quantum cascade laser design for the mid-IR and THz spectral range. Appl. Phys. A **109**, 763–768 (2012). https://doi.org/10.1007/s00339-012-7343-2

Schurig, D., Mock, J.J., Justice, B.J., Cummer, S.A., Pendry, J.B., Starr, A.F., Smith, D.R.: Metamaterial electromagnetic cloak at microwave frequencies. Science **314**, 977–980 (2006). https://doi.org/10.1126/science.1133628

Shalaev, V.M.: Optical negative-index metamaterials. Nat. Photon. **1**, 41–48 (2007). https://doi.org/10.1038/nphoton.2006.49

Shelby, R. A., Smith, D. R., Schultz, S.: Experimental verification of a negative index of refraction. Science **292**, 77–79 (2001). https://doi.org/10.1126/science.1058847

Smiljanić, J., Žeželj, M., Milanović, V., Radovanović, J., Stanković, I.: MATLAB-based program for optimization of quantum cascade laser active region parameters and calculation of output characteristics in magnetic field. Comput. Phys. Commun. **185**, 998–1006 (2014). https://doi.org/10.1016/j.cpc.2013.10.025

Thongrattanasiri, S., Podolskiy, V.A.: Hypergratings: nanophotonics in planar anisotropic metamaterials. Opt. Lett. **34**, 890–892 (2009). https://doi.org/10.1364/OL.34.000890

Unuma, T., Takahashi, T., Noda, T., Yoshita, M., Sakaki, H., Baba, M., Akiyama, H.: Effects of interface roughness and phonon scattering on intersubband absorption linewidth in a GaAs quantum well. Appl. Phys. Lett. **78**, 3448–3450 (2001). https://doi.org/10.1063/1.1376154

Vitiello, M.S., Scalari, G., Williams, B., De Natale, P.: Quantum cascade lasers: 20 years of challenges. Opt. Express **23**, 5167–5182 (2015). https://doi.org/10.1364/OE.23.005167

Vuković, N., Milanović, V., Radovanović, J.: Influence of nonparabolicity on electronic structure of quantum cascade laser. Phys. Lett. A **378**, 2222–2225 (2014a). https://doi.org/10.1016/j.physleta.2014.04.069

Vuković, N., Radovanovic, J., Milanovic, V.: Enhanced modeling of band nonparabolicity with application to a mid-IR quantum cascade laser structure. Phys. Scr. **T162**, 014014 (2014b). https://doi.org/10.1088/0031-8949/2014/T162/014014

Vuković, N., Daničić, A., Radovanović, J., Milanović, V., Indjin, D.: Possibilities of achieving negative refraction in QCL-based semiconductor metamaterials in the THz spectral range. Opt. Quantum Electron. **47**, 883–891 (2015). https://doi.org/10.1007/s11082-014-0020-2

Wacker, A.: Quantum cascade laser: an emerging technology. In: Nonlinear Laser Dynamics, Berlin (2012)

Westmeyer, A.N., Mahajan, S., Bajaj, K.K., Lin, J.Y., Jiang, H.X., Koleske, D.D., Senger, R.T.: Determination of energy-band offsets between GaN and AlN using excitonic luminescence transition in AlGaN alloys. J. Appl. Phys. **99**, 013705 (2006). https://doi.org/10.1063/1.2158492

Zhou, J., Koschny, T., Kafesaki, M., Economou, E.N., Pendry, J.B., Soukoulis, C.M.: Saturation of the magnetic response of split-ring resonators at optical frequencies. Phys. Rev. Lett. **95**, 223902 (2005). https://doi.org/10.1103/PhysRevLett.95.223902